Dynamics of phonons in submicrometer zones generated by an optical waveguide

R. J. van Wijk, J. I. Dijkhuis, and H. W. de Wijn
Faculty of Physics and Astronomy, and Debye Research Institute, University of Utrecht, P.O. Box 80000, 3508 TA Utrecht, The Netherlands
(Received 23 October 1990)

We introduce a technique utilizing the evanescent field of an optical waveguide to examine the dynamics of nonequilibrium high-frequency phonons resonant with optically excited centers in zones of submicrometer dimension. The technique is used to create a nearly saturated zone of excited Cr^{3+} ions at the surface of a 700-at. ppm ruby crystal at 1.5 K by optical pumping through the broad bands. At the same time, the optical pumping serves to generate resonant 29-cm^{-1} phonons. The decay of the combined spin-phonon system, measured via the R_2 luminescence following interruption of the optical pumping, is explained by elastic spatial diffusion in parallel with spectral wipeout. The time constant for loss by spatial diffusion is derived rigorously from rate equations. Spectral wipeout is treated according to the model developed by Goossens *et al.* based on one-site inelastic scattering by weakly exchange-coupled Cr^{3+} pairs, but modified to include the appreciable elastic diffusion remaining after wipeout under the present extreme conditions. Spectral wipeout turns out to predominate at high excited-state concentration. The optical feeding into $2\overline{A}(^2E)$ is found to result mainly from excited-state absorption starting from $\overline{E}(^2E)$, despite the low probability of the latter at the light wavelength used (514.5 nm).

I. INTRODUCTION

Resonant trapping of nonequilibrium high-frequency phonons (29 cm^{-1}, 0.87 THz) by optically excited Cr^{3+} in ruby has been studied extensively.[1] In particular, insight has been gained into the processes that govern the ultimate disappearance of resonant phonons from the excited zone. The decay of these phonons can be observed via the R_2 luminescence by taking advantage of the dynamical equilibrium between resonant phonons and the excited Cr^{3+}. At low excited-ion concentrations N^*, or small zone dimensions, the phonons escape by spatial diffusion towards the border of the excited zone. The resonant phonon lifetime then is governed by N^* through the phonon mean free path on the one hand and by the net distance L the phonons must travel towards the border of the excited zone on the other. In fact, the product N^*L is the parameter determining the resonant phonon lifetime, provided N^* is many times larger than the density of resonant phonon modes $\rho\Delta\nu$.

At high N^*, or large zone dimensions, spatial diffusion is too ineffective a mechanism for phonon escape. The phonons are more likely to undergo a frequency shift away from resonance by inelastic scattering,[2–5] after which they can leave the excited zone undisturbed. Goossens, Dijkhuis, and de Wijn[4] proposed that one-site Raman scattering by weakly exchange-coupled Cr^{3+} pairs is the relevant frequency shifting mechanism. A marked characteristic of this mechanism is that the frequency shifts involved are comparable to the linewidth of the resonant phonon line. This implies that it is the size of the zone in relation to the modified mean free path that determines whether a frequency shift is large enough for the shifted phonon to leave the excited zone. Apart from N^*, therefore, L is again a parameter relevant to the resonant phonon lifetime, and, if $N^* \gg \rho\Delta\nu$, the lifetime is again dependent only on their product N^*L. This was demonstrated in Ref. 4 for zone dimensions varying by an order of magnitude upwards from 60 μm.

The purpose of this paper is to investigate to what extent the complementary role of N^* and L persists when these parameters attain extreme values. The evanescent field of a guided mode of an optical waveguide is used to create an essentially saturated excited zone of submicrometer dimension at the surface of a bulk ruby crystal at 1.5 K. The evanescent field decreases exponentially with the depth, with a characteristic length of the order of 100 nm. Due to the compression in the vertical dimension, the energy density in the guided mode is several orders of magnitude larger than in a focused laser beam. The imprisonment of phonons resonant with the $2\overline{A}(^2E)-\overline{E}(^2E)$ transition in Cr^{3+} is subsequently measured as a function of time under these exceptional conditions of large N^* and small L. In analyzing the results, it appears feasible to treat the spatially diffusive part of the phonon escape to a substantial degree of exactness. Further, it is necessary to reconsider the criterion for the escape of frequency-shifted phonons. After having done this, however, it turns out that N^*L remains the relevant parameter, and that the mechanism of wipeout by one-site Raman scattering off exchange-coupled pairs combined with spatial diffusion adequately accounts for the experiments.

II. EXPERIMENT

A planar optical waveguide, i.e., a dielectric film of optical-wavelength thickness on top of a substrate with a lower refractive index,[6-8] was used to create a submicrometer zone of Cr^{3+} excited to $\overline{E}(^2E)$ by optical pumping via the broad bands at the surface of a bulk ruby crystal. The ruby crystal was a Czochralsky-grown slab with a Cr^{3+} concentration of 700-at. ppm, measuring $2 \times 2 \times 0.1$ cm^3. The c axis was oriented perpendicular to the larger faces. The latter were optically polished, and a siliconoxynitride film (thickness 278 nm, index of refraction 1.86) was deposited on one of them by plasma-enhanced chemical vapor deposition. Light from an argon ion laser, operating in the single-line mode at 514.5 nm, was coupled into the waveguide through a 45°–90°–45° prism of SF59 glass, which was held pressed against the waveguide by a phosphor-bronze blade spring. In the technique of prism coupling, light tunnels through the low-refractive-index gap, sized a fraction of a wavelength, between prism and waveguide.[8,9] At the wavelength used, the waveguide only supports the TE_0 and TM_0 modes. (For TE modes the electric field is linearly polarized parallel to the surface, while for TM modes the polarization is elliptical in the sagittal plane.) Some properties of these modes under the present conditions are listed in Table I. At the optimum angle of incidence the laser beam is nearly parallel to the sample surface. Sample and prism were immersed in superfluid liquid helium at 1.5 K to freeze out thermally activated relaxation. The sample was positioned with the film upright to provide optical access to the sample surface at right angles to the laser beam and to facilitate adjustment of the angle of incidence.

The development of the nonequilibrium population of 29-cm^{-1} phonons was repetitively monitored via the R_2 luminescence emanating from the excited zone following interruption of the optical pumping with an acousto-optical modulator. The luminescence was collected at near right angles to the film. The receiving optics confined the area of detection to about 5 mm along the guided light. Special care was taken to mask the spot where the laser beam couples into the film because the associated stray light produces a substantial excitation of bulk ruby. The luminescence was analyzed by use of a 0.85-m double monochromator, and time-to-amplitude conversion followed by pulse-height analysis provided the necessary resolution in time.

III. MODEL

A. Excited zone

First, we model the profile of the excited zone generated at the ruby surface by the evanescent field. The power density of the evanescent wave in the substrate at a distance z from the film-substrate interface is

$$w(z) = \frac{fW}{l_0 B} \exp(-z/l_0) , \tag{1}$$

in which W is the laser power coupled into the guided mode, f the fraction of the guided-mode power carried by the substrate, l_0 the intensity penetration depth, and B the width of the guided beam. In the case of pumping via the broad bands, the local excited-ion concentration $N^*(z)$ can be written $N^*(z) = N_0 w(z)/[w(z) + w_h]$, where N_0 is the concentration of Cr^{3+} ions and w_h the power density exciting half of N_0. Upon introducing the ratio of power densities $A = w_h B l_0 / fW$, therefore,

$$N^*(z) = \frac{N_0}{1 + A \exp(z/l_0)} . \tag{2}$$

For the TE_0 mode, $A = 0.024$ for the typical values $w_h = 6$ kW/cm^2, $B = 100$ μm, and $W = 100$ mW. In Eq. (2), any effects from stimulated emission due to population inversion of $\overline{E}(^2E)$ relative to $^4A_2$ at high power densities have been ignored. Also ignored is redistribution of $N^*(z)$ due to reabsorption of R_1 luminescence within the zone on the grounds that the zone thickness is many orders of magnitude smaller than the mean free path of R_1 light in ruby.

As is seen in Fig. 1, the profile of $N^*(z)$ resulting from Eq. (2) in general exhibits a region of near saturation with a slowly varying $N^*(z)$, followed by a gradual decrease in $N^*(z)$, and finally an exponential tail. Note that an increase in the laser power results in an expansion of the excited zone in space rather than a change in $N^*(z)$ in the region of saturation. This is in contrast with conventional bulk experiments employing a focused laser beam. Integration of $N^*(z)$ over the depth yields

$$N^* d = N_0 l_0 \ln(1 + 1/A) . \tag{3}$$

TABLE I. Guided-mode parameters. Angles of incidence are relative to the film normal.

	TE_0	TM_0
Angle of incidence in film (deg)	74.2	73.1
Fraction of power in substrate f	0.38	0.55
Intensity penetration depth l_0 (nm)	155	218
Angle of incidence in air (deg)	88.1	86.4
Polarization	E⊥c	E∥c [a]

[a] Long axis. Ratio of long to short axis is 9.6.

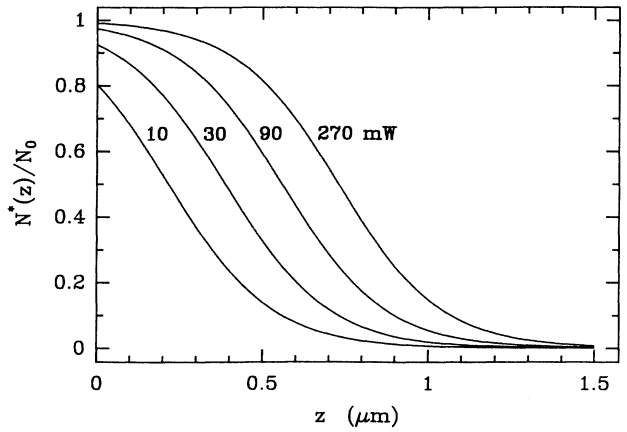

FIG. 1. The excited-ion concentration N^*, normalized to N_0, vs the distance z from the film-substrate interface for several guided-mode powers W, as indicated. Guided mode is TE_0. Zone width $B = 0.1$ mm; $w_h = 6$ kW/cm^2.

Here, the integral is symbolically denoted as N^*d, since it may be thought of as the product of a constant N^* and an effective depth of the zone. As such, it is closely related to the product N^*L in the earlier experiments on the phonon bottleneck.

B. Phonon loss mechanisms

1. Spatial diffusion

In this section, we derive an expression for the relaxation time $T_{\rm dif}$ associated with spatial diffusion of the resonant phonons towards the zone boundary by multiple elastic scattering by Cr^{3+} ions, i.e., we ignore all processes leading to a frequency shift. As to the geometry, the problem is assumed to depend only on the depth below the waveguide on the grounds that the zone width ($B \sim 100$ μm) is much larger than the typical zone depth (< 1 μm). We further neglect radiative decay of $2\overline{A}(^2E)$ and $\overline{E}(^2E)$ to the $^4A_2$ ground state ($\tau_R = 3.7$ ms), since it is three orders of magnitude slower than the time scale of our experiments. The rate equations governing the spatial and temporal development of the $2\overline{A}(^2E)$ population $N_{2\overline{A}}(z,t)$ and the phonon occupation number p can then be written

$$\frac{\partial N_{2\overline{A}}(z,t)}{\partial t} = -\frac{[p(z,t)+1]N_{2\overline{A}}(z,t)}{T_d} + \frac{p(z,t)N_{\overline{E}}(z)}{T_d} + \phi(z)\eta(t) \ , \tag{4}$$

$$\rho\Delta\nu\frac{\partial p(z,t)}{\partial t} = \frac{[p(z,t)+1]N_{2\overline{A}}(z,t)}{T_d} - \frac{p(z,t)N_{\overline{E}}(z)}{T_d} + \rho\Delta\nu\frac{\partial}{\partial z}\left(D(z)\frac{\partial p(z,t)}{\partial z}\right) \ , \tag{5}$$

where $N_{\overline{E}}(z)$ is the concentration of Cr^{3+} maintained in $\overline{E}(^2E)$, $\rho\Delta\nu$ is the density of resonant phonon modes, T_d is the lifetime of $2\overline{A}(^2E)$ against one-phonon decay to $\overline{E}(^2E)$, $D(z)$ is the diffusion constant, and $\phi(z)$ represents the optical feeding into $2\overline{A}(^2E)$. Note that $N_{\overline{E}}(z) + N_{2\overline{A}}(z) = N^*(z)$. The function $\eta(t)$ occurring in Eq. (4) equals unity during the optical feeding, and zero otherwise. The diffusion constant $D(z)$ is defined by the kinetic expression $D(z) = \frac{1}{3}\Lambda(z)v$, where v is the velocity of sound, and $\Lambda(z)$ is the phonon mean free path against reabsorption. Since $N_{2\overline{A}}(z) \ll N_{\overline{E}}(z)$, we have

$$\Lambda(z) = \rho\Delta\nu v T_d/N^*(z) \ . \tag{6}$$

It is noted that $\Lambda(z)$ is small relative to the distances associated with variation of $N^*(z)$. For instance, $\Lambda(z)$ amounts to 5 nm for $N^*(z) \simeq N_0$. At depths where $N^*(z)$ has dropped to low values, however, $\Lambda(z)$ deviates from Eq. (6) by becoming smaller in the direction of the interface and larger away from it. Examination of these effects, however, indicates that the use of Eq. (6) at all depths only negligibly overestimates the final result for $T_{\rm dif}$ below.

We first solve the equations in the absence of optical feeding [$\eta(t) = 0$]. By summing Eqs. (4) and (5), adopting the condition of dynamical equilibrium $N_{2\overline{A}}(z) = p(z)N_{\overline{E}}(z)/[p(z)+1] \approx p(z)N^*(z)$, and finally substituting Eqs. (2) and (6), we arrive at a partial differential equation that can be solved analytically by separation of variables. Upon introducing $x = z/l_0$, the solutions are $p(x,t) = X(x)\exp(-\lambda^2 t/\tau_0)$, where

$$\tau_0 = \frac{3(N_0 l_0)^2}{(\rho\Delta\nu v)^2 T_d} \tag{7}$$

and where $X(x)$ is a solution of

$$\frac{d^2X}{dx^2} + \frac{Ae^x}{1+Ae^x}\frac{dX}{dx} + \left(\frac{\rho\Delta\nu/N_0}{1+Ae^x} + \frac{1}{(1+Ae^x)^2}\right)\lambda^2 X(x) = 0 \ . \tag{8}$$

We ignore the term containing $\rho\Delta\nu/N_0 \sim 10^{-3}$, since it contributes significantly only in regions where $N^*(z)$ and $p(z,t)$ have dropped to negligible values. The solutions of Eq. (8) then are $X(x) = a\sin[\lambda y(x) + b]$, with

$$y(x) = \ln\left(\frac{1+A}{e^{-x}+A}\right) \ . \tag{9}$$

The variable $y(x)$ can be regarded a new space coordinate, measuring the depth in terms of the mean free path, i.e., $dy/dx \propto 1/\Lambda(x)$. While x ranges from zero to infinity, y ranges from zero to $y_\infty = \ln(1+1/A) = N^*d/N_0 l_0$. In terms of $y(x)$ we are therefore dealing with a finite system, so that only discrete values of λ occur in the general solution for $p(x,t)$. The latter can thus be written

$$p(x,t) = \sum_{n=0}^{\infty} a_n \sin[\lambda_n y(x) + b_n]\exp(-\lambda_n^2 t/\tau_0) \ . \tag{10}$$

The coefficients a_n and b_n have to be determined from Fourier analysis of the initial distribution $p_0(x) = p(x,0)$ with the optical feeding turned on [$\eta(t) = 1$]. Since in our experiments the optical feeding persists long enough to reach a stationary distribution of p, we solve Eqs. (4) and (5) with the time derivatives set to zero. Further, in anticipation of the discussion of the various mechanisms of optical feeding, the optical feeding into $2\overline{A}(^2E)$ is assumed to be proportional to the local $N^*(z)$, i.e., $\phi(z) = \psi N^*(z)$, with ψ independent of the depth. The equation for $p_0(x)$ then becomes

$$\frac{d^2p_0(x)}{dx^2} + \frac{Ae^x}{1+Ae^x}\frac{dp_0(x)}{dx} + \frac{\psi\tau_0}{(1+Ae^x)^2} = 0 , \qquad (11)$$

which, upon incorporating the boundary condition that $p_0 = 0$ for $x \to \infty$, is solved by

$$p_0(x) = \psi\tau_0\{\tfrac{1}{2}[y_\infty^2 - y^2(x)] - c[y_\infty - y(x)]\} . \qquad (12)$$

The integration constant c is, in turn, found from the boundary condition at $x = 0$. The latter depends on the phonon reflection coefficient R at the substrate-film interface. In the absence of reflection ($R = 0$), we simply have $p(0) = 0$, or $c = y_\infty/2$. For total reflection ($R = 1$), on the other hand, the flow through the interface vanishes, whence $-D(0)dp/dz = 0$ and $c = 0$.

In the case $R = 0$, we carry out the Fourier analysis of p_0 upon adopting an antisymmetric continuation of p_0 beyond the interval $[0, y_\infty]$ to ensure that $p \to 0$ for $t \to \infty$. The results are $\lambda_n = n\pi/y_\infty$, $a_n = 4\psi\tau_0/\lambda_n^3 y_\infty$, and $b_n = 0$ for odd n; for even n, $a_n = 0$. In the experiments, the phonon population is not monitored directly, but via detection of the R_2 luminescence. The latter is proportional to $N_{2\overline{A}}(z) = p(z)N^*(z)$ integrated over the depth over the zone. The integration yields

$$\overline{N}_{2\overline{A}} = 8\psi\tau_0 N_0 l_0 y_\infty^3 \times \sum_{n=0}^{\infty} \frac{\cos[\lambda_{2n+1}\ln(A)]}{[(2n+1)\pi]^4}\exp(-\lambda_{2n+1}^2 t/\tau_0) . \qquad (13)$$

The decay time of the leading term is

$$T_{\rm dif} = \frac{3(N^*d)^2}{\pi^2(\rho\Delta\nu v)^2 T_d} . \qquad (14)$$

The second term, which decays nine times faster, has an amplitude of less than 4% of that of the first term in the range of guided-mode powers used ($A < 1$). It is noted that $T_{\rm dif}$ equals the leading decay time in a slab of uniform $N^*(z)$ and thickness L, if the identification $N^*L = N^*d$ is made.[10]

Quite remarkably, Eq. (14), which is derived for spatial diffusion in the case $R = 0$, holds for any R encountered in the present experiments ($R \lesssim 0.8$). To explain this, we consider the boundary condition at $x = 0$ for arbitrary R. The gross phonon flow F_g incident on the substrate-film interface is to a good approximation given by[11]

$$F_g = \frac{\rho\Delta\nu v}{2\Lambda(0)}\int_0^\infty dr \int_0^{\pi/2} d\theta\; p(z)\sin\theta\cos\theta\exp[-r/\Lambda(0)] , \qquad (15)$$

where $z = r\cos\theta$. The phonon flow through the interface equals $-(1-R)F_g$. Relating this to the net flow F_n occurring in the diffusion equation is a notorious problem.[12] Writing $F_n = -f_R D(0)\rho\Delta\nu(\partial p/\partial z)_{z=0}$, we have $f_R = 1$ for the limiting case $R \sim 1$, as in the bulk, but $f_R = \frac{1}{2}$ for $R = 0$ because of the absence of a diffusive medium at the other side of the interface. By expansion of p to first order in z and performing the integrations in Eq. (15), we obtain for the boundary condition the quite general result

$$\left(\frac{1}{p}\frac{\partial p}{\partial z}\right)_{z=0} = \frac{3}{2\Lambda(0)}\frac{1-R}{2f_R - 1 + R} . \qquad (16)$$

We henceforth adopt the linear interpolation $f_R = \frac{1}{2}(1+R)$. Further expansion of p in z results in negligible corrections except at the transition from the diffusive to the ballistic regime. Rewriting the boundary condition in terms of $y(x)$, and applying the result to p_0 in Eq. (12), we find

$$c = \tfrac{1}{2}y_\infty\frac{\gamma y_\infty}{1+\gamma y_\infty} , \qquad (17)$$

where

$$\gamma = \frac{3N_0 l_0}{2\rho\Delta\nu v T_d}\frac{1-R}{2R} . \qquad (18)$$

In our experiments, $\gamma = 28(1-R)/R$ for the TE_0 mode and $40(1-R)/R$ for the TM_0 mode, while y_∞ typically ranges between 2 and 5. We thus see that c approximates the value $\frac{1}{2}y_\infty$ corresponding to $R = 0$, except when R is near unity.

2. Spectral wipeout

At high N^*L, the resonant phonons are so severely trapped within the zone that spatial diffusion towards the zone boundary becomes ineffective. Rather, the phonons escape after undergoing a frequency shift away from resonance, resulting in a substantial enlargement of the mean free path.[2-4] Goossens, Dijkhuis, and de Wijn[4] have suggested that these shifts occur by one-site inelastic scattering by weakly exchange-coupled Cr^{3+} pairs, and have quantified this in an approximate, but analytical, treatment. Here, we first recapitulate the essential ingredients of this treatment as far as is relevant to the present discussion.

Due to the exchange, the $2\overline{A}(^2E)$ and $\overline{E}(^2E)$ Kramers doublets are each split. In the molecular-field approximation, both splittings equal the $\overline{E}(^2E) - {}^4A_2$ exchange parameter J, which strongly depends on the distance to the nearest Cr^{3+} in the ground state. Upon adopting a random distribution of Cr^{3+} ions over space, and a J depending on distance as $J = J_0\exp(-ar)$,[13,14] the distribution D_J of Cr^{3+} ions with a splitting between J and $J + dJ$ reads, normalized to $\int_0^\infty D_J dJ = 1$,

$$D_J = \frac{4\pi N_0[\ln(J/J_0)]^2}{a^3 J} \exp\left(\frac{4\pi N_0[\ln(J/J_0)]^3}{3a^3}\right) . \tag{19}$$

The quantities J_0 and a amount to 330 cm^{-1} and 1 $Å^{-1}$, respectively.[2,4,13] For the case of 700-at. ppm ruby, the function D_J is shown in Fig. 2. The two splittings being equal, the two spin-nonflip transitions connecting $2\overline{A}(^2E)$ and $\overline{E}(^2E)$ remain at resonance with the phonons. A phonon absorbed in a spin-nonflip transition to $2\overline{A}(^2E)$ may be shifted in frequency by J when reemitted in a spin-flip transition back to $\overline{E}(^2E)$. This occurs in $T_d/T_d^{(f)} \approx 6\%$ of the scattering events, with $T_d^{(f)}$ denoting the spin-flip one-phonon decay time of $2\overline{A}(^2E)$.

A shifted phonon may return to resonance by the reverse process, i.e., a spin-flip capture by a Cr^{3+} with the appropriate splitting followed by spin-nonflip emission, if the mean free path at the displaced frequency,

$$\Lambda_{\rm inel}(J) = 2\rho T_d^{(f)} v/D_J N^* , \tag{20}$$

is still smaller than the average flight path L out of the excited zone. However, in the event that the frequency shift is large enough, the phonon will, on the average, leave the zone instead of returning to resonance. An interruption involving a shift of sufficient size is called a one-step spectral wipeout, and the minimum shift resulting in wipeout $J_{\rm crit}$.

In the model, the Cr^{3+} ions are, for tractability, divided into two classes. The first class (type I) is formed by Cr^{3+} having splittings too small to produce wipeout. The associated frequency shifts are ignored. The remaining Cr^{3+}, capable of inducing wipeout, are lumped together in a second class (type II). They provide an energy leakage of the form [cf. Eq. (8) of Ref. 4]

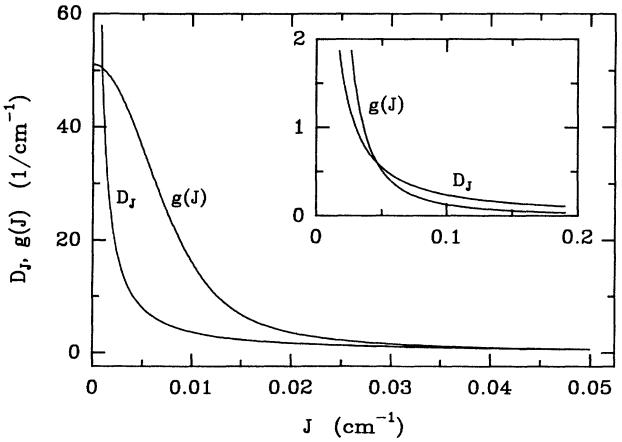

FIG. 2. The distribution D_J of exchange splittings of Cr^{3+} and the resonant line shape $g(J)$ of $\overline{E}(^2E)-2\overline{A}(^2E)$ in 700-at. ppm ruby.

$$(N^* + \rho\Delta\nu)\frac{dp}{dt} = -\alpha N_{2\overline{A}}^{\rm II}/T_d^{(f)} , \tag{21}$$

where the parameter α accounts for a reduction, relative to type I, of the coupling of type-II Cr^{3+} with the unshifted phonons due to a broadening of the $\overline{E}(^2E)-2\overline{A}(^2E)$ transition with increasing J. Equation (21) combined with the notion that the type-II Cr^{3+} by themselves are in dynamical equilibrium with the phonons, i.e., $p \approx N_{2\overline{A}}^{\rm II}/N^{\rm II*}$, yields an effective relaxation time for removal by wipeout

$$T_w = T_d^{(f)}(N^* + \rho\Delta\nu)/\alpha N^{\rm II*} . \tag{22}$$

The concentration of type-II Cr^{3+} ions, $N^{\rm II*}$, is in turn found by integrating D_J for $J > J_{\rm crit}$, with the result

$$\frac{N^{\rm II*}}{N^*} = 1 - \exp\left(\frac{4\pi N_0[\ln(J_{\rm crit}/J_0)]^3}{3a^3}\right) . \tag{23}$$

We now turn to an estimation of $J_{\rm crit}$, the minimum shift resulting in spectral wipeout. This will lead to a new criterion for wipeout valid under the present condition of small to moderate N^*L. In the cases studied in Ref. 4, i.e., optically excited zones of medium N^* ranging from 60–600 μm in diameter, N^*L typically was of order 10^{16} cm^{-2} or larger. The majority of the exchange-induced frequency shifts then carry the phonons well into the wings of the spin-nonflip phonon transition, which has a width $\Delta\nu = 0.015$ cm^{-1}.[15] Accordingly, the criterion for wipeout could be adequately approximated by demanding that $\Lambda_{\rm inel}(J)$ exceed the radius of the exciting laser beam, which indeed is a reasonable measure of the average path L to the zone boundary in ballistic flight. In the present experiments, by contrast, $N^*L \simeq N^*d \simeq 10^{15}$ cm^{-2}. In 700-at. ppm ruby at these low N^*L, frequency shifts satisfying the criterion $\Lambda_{\rm inel}(J) \gtrsim L$ may be as small as 0.002 cm^{-1}, substantially smaller than the width of the spin-nonflip transition. Shifts satisfying this criterion, therefore, do not necessarily free a resonant phonon from trapping by the *spin-nonflip* transitions of type-I Cr^{3+} and, for that matter, type-II Cr^{3+}. In other terms, at the low N^*L encountered here the criterion for wipeout must be refined so as to account for the appreciable diffusive motion by elastic reabsorption and reemission over the unshifted transitions. In a sufficiently accurate approximation, the mean free path against these processes is given by [cf. Eq. (6)]

$$\Lambda_{\rm el}(J) = \rho T_d v/g(J)N^* , \tag{24}$$

in which $g(J)$ is the line shape of the $\overline{E}(^2E)-2\overline{A}(^2E)$ transition (Fig. 2). It is noted that the ratio $\Lambda_{\rm inel}/\Lambda_{\rm el}$ amounts to $2T_d^{(f)}g(J)/T_d D_J \sim 30g(J)/D_J$, given that $T_d = 0.7$ ns (Refs. 15 and 16) and $T_d^{(f)} \approx 12$ ns.

To formulate a new criterion for wipeout, we consider the mean number n of elastic scattering events suffered by a phonon prior to leaving the excited zone once it has been shifted from resonance by an amount J. In the case

of a uniformly excited slab of thickness h, we have for the leading mode of the decay $n = (3/\pi^2)(h/\Lambda_{el})^2$ (cf. Ref. 10) or, upon noting that averaged over all directions $L = h$, $n = (3/\pi^2)(L/\Lambda_{el})^2$. For a uniformly excited cylinder of radius R, the analogous expressions are $L = 4R/\pi$ and $n = (3/5.783)(\pi/4)^2(L/\Lambda_{el})^2$. For any geometry, therefore,

$$n \approx 0.3(L/\Lambda_{el})^2 \ . \tag{25}$$

To ensure that, on the average, a phonon does not return to resonance after a shift of magnitude J, we must have $\Lambda_{inel}(J) \gtrsim n\Lambda_{el}(J)$. So the new criterion for wipeout inclusive of elastic diffusive motion remaining after small shifts can be written

$$[\Lambda_{el}(J)\Lambda_{inel}(J)]^{1/2} \gtrsim 0.5\,L \ . \tag{26}$$

The left-hand side of Eq. (26) is inversely proportional to N^*. As in the case of the earlier criterion $\Lambda_{inel}(J) \gtrsim L$,[4] therefore, T_w depends on the parameters N^* and L only through their product N^*L provided, of course, $N^* \gg \rho\Delta\nu \approx 3.2 \times 10^{16}$ cm^{-3}.

C. Feeding mechanisms

The optical feeding serves to create the resonant phonons by direct decay from $2\overline{A}(^2E)$ to $\overline{E}(^2E)$ following pumping into $2\overline{A}(^2E)$, and further to maintain the excited zone. In the derivation of Eq. (14), it has been assumed that, under stationary conditions, the feeding is proportional to the local $N^*(z)$. This assumption needs some justification, since secondary optical pumping starting from $\overline{E}(^2E)$ and relaxation of near-zone-boundary phonons generated in the optical pumping cycles may significantly add to the feeding.[17] Furthermore, a comparison of the signal intensity in relation to the guided-mode power permits identification of the dominant feeding mechanism.

The optical feeding of $2\overline{A}(^2E)$ results from four processes, which are depicted schematically in Fig. 3. We first consider the primary optical pumping cycle from the $^4A_2$ ground state via the $^4T_2$ broad band. Its rate is proportional to the local laser power density $w(z)$ and the concentration $N_0 - N^*(z)$ of the $^4A_2$ ground state. Furthermore, under stationary or quasi-stationary conditions, the local pumping to ^2E as a whole balances the local return to $^4A_2$. That is, at a depth z in the excited zone,

$$\alpha_1 w(z)[N_0 - N^*(z)] = N^*(z)/\tau_R \ , \tag{27}$$

where α_1 is the absorption coefficient. The primary pumping into $2\overline{A}(^2E)$, which equals the total feeding into ^2E times the branching ratio $\beta_1 = \phi_{2\overline{A}}/(\phi_{2\overline{A}} + \phi_{\overline{E}}) = 0.007$,[17] thus amounts to

$$\phi_1(z) = \frac{\beta_1}{\tau_R} N^*(z) \ . \tag{28}$$

A second mechanism of feeding into $2\overline{A}(^2E)$ is redistribution between the populations of $2\overline{A}(^2E)$ and $\overline{E}(^2E)$ by Raman processes induced by zone-boundary phonons. The latter are created as a product of the optical pumping cycle during the nonradiative decay from the broad bands to $\overline{E}(^2E)$ and $2\overline{A}(^2E)$, and similarly by the nonradiative decay following excited-state absorption of laser light starting from $\overline{E}(^2E)$ to near the $^2T_1'$ state at 32 400 cm^{-1}.[17] The rate of the latter process is

$$\alpha_2 w(z) N^*(z) = \frac{\alpha_2}{\alpha_1 \tau_R} \frac{[N^*(z)]^2}{N_0 - N^*(z)} \ , \tag{29}$$

where α_2 is the absorption coefficient for excited-state absorption from ^2E, and as in Eq. (27) the right-hand side applies to stationary pumping. From Ref. 18 we find that, at 103 K, $\alpha_2/\alpha_1 = 5/11$ for pumping through TE_0 and $\alpha_2/\alpha_1 = 4/5$ for pumping through TM_0. According to Eq. (29), the generation of zone-boundary phonons is highly position dependent, and highest near the film-substrate interface. However, the mean free path of zone-boundary phonons against absorption by $2\overline{A}(^2E)$ or $\overline{E}(^2E)$ is of the order of 100 μm or larger, even in the event of complete inversion of these levels relative to the ground state.[17] This, in effect, yields a uniform distribution of the generated zone-boundary phonons over the optically excited region. To calculate the *local* feeding into $2\overline{A}(^2E)$ invoked by zone-boundary phonons, therefore, the rate of generation of these phonons must be averaged over the excited zone prior to calculating the rate of scattering by Raman processes.

The energy surplus of the decay from $^4T_2$ to ^2E amounts to 5025 cm^{-1}, compared to an energy of $\sim$230 cm^{-1} per zone-boundary phonon. In each cycle of the primary pumping, therefore, approximately 5025/230 zone-boundary phonons are created, which are distributed over roughly $3N_{prim}$ modes, where $N_{prim} = 1.1 \times 10^{22}$ cm^{-3} is the number of primitive cells. These phonons travel at an average speed $v_{ZB} \approx 10^5$ cm/s. Multiplying by the rate of the primary pumping cycle $N^*(z)/\tau_R$, and integrating over the zone, we then find for the contribution of the primary pumping cycle to the occupation number of the zone-boundary phonons ($R \sim 0$)

$$p_{ZB,1} = \frac{1}{3N_{prim} v_{ZB} \tau_R} \frac{5025}{230} N^* d \ . \tag{30}$$

The resultant net rate of the Raman processes from $\overline{E}(^2E)$ to $2\overline{A}(^2E)$ at any site is $p_{ZB,1}[N_{\overline{E}}(z) - N_{2\overline{A}}(z)]/T_{Ram}$, where $T_{Ram} \approx 10^{-10}$ s.[19] As $N_{2\overline{A}}(z) \ll N_{\overline{E}}(z) \approx N^*(z)$, we have for the local Raman-feeding rate by zone-boundary phonons generated in the primary pumping cycle

$$\phi_2(z) = \frac{\beta_2}{\tau_R} \frac{5025}{230} N^* d N^*(z) \ , \tag{31}$$

in which $\beta_2 = 1/(3N_{prim} T_{Ram} v_{ZB})$, and, as before, N^*d should be regarded a single quantity.

The contribution of the excited-state absorption to the zone-boundary phonon occupation and the associated Raman-induced feeding are similarly found by integrat-

ing the right-hand side of Eq. (29) over the depth of the zone, and noting that about 19 445/230 zone-boundary phonons are created in each secondary pumping cycle. The results are

$$p_{\mathrm{ZB},2} = \frac{1}{3N_{\mathrm{prim}} v_{\mathrm{ZB}} \tau_R} \frac{19\,455}{230} \frac{\alpha_2}{\alpha_1} \left(\frac{N_0 l_0}{A} - N^* d \right) , \tag{32}$$

and

$$\phi_3(z) = \frac{\alpha_2 \beta_2}{\alpha_1 \tau_R} \frac{19\,455}{230} \left(\frac{N_0 l_0}{A} - N^* d \right) N^*(z) . \tag{33}$$

The total rate of the Raman feeding, of course, amounts to the sum of ϕ_2 and ϕ_3. Note that, by virtue of the long mean free path of zone-boundary phonons, both Raman-associated processes do indeed scale linearly with $N^*(z)$.

In addition to the above three feeding mechanisms, excited-state absorption starting from $\overline{E}(^2E)$ causes a direct redistribution over $2\overline{A}(^2E)$ and $\overline{E}(^2E)$ to the extent that the ensuing nonradiative decay from $^2T_1'$ terminates in $2\overline{A}(^2E)$ (mechanism 4 in Fig. 3). This mechanism of redistribution among the ^2E levels has not been considered before as it is negligible compared to the Raman feeding in conventional excited zones. In the present experiments, however, it has gained importance because the efficiency of the Raman mechanisms is reduced by the small zone dimension, and the excited-state absorption is greatly enhanced at the high N^* and laser-power densities achieved. The rate of the direct redistribution by excited-state absorption, of course, scales with the secondary pumping rate, Eq. (29). It is furthermore reasonable to assume that the final part of the nonradiative decay from $^2T_1'$ down to ^2E passes through the same states as the nonradiative decay following the primary pumping cycle, i.e., $^4T_2$ and $^2T_1$, the latter of which is situated between $^4T_2$ and ^2E. We therefore adopt the same branching ratio β_1 over $2\overline{A}(^2E)$ and $\overline{E}(^2E)$, to obtain for the local rate of the direct redistribution by the excited-state absorption

$$\phi_4(z) = \frac{\alpha_2 \beta_1}{\alpha_1 \tau_R} \frac{[N^*(z)]^2}{N_0 - N^*(z)} . \tag{34}$$

To compare the contributions of the four mechanisms to the total feeding into $2\overline{A}(^2E)$, we calculate, for each process, the average feeding into $2\overline{A}(^2E)$ per excited Cr^{3+} ion, or

$$\psi_i = \int_0^\infty \phi(z) dz \Big/ \int_0^\infty N^*(z) dz . \tag{35}$$

Noting that $\int_0^\infty N^*(z) dz = N^* d$, we find ψ_i for the first three processes from $\phi_i(z)$ by replacing $N^*(z)$ in the relevant expressions by unity. For the fourth process we find

$$\psi_4 = \frac{\alpha_2 \beta_1}{\alpha_1 \tau_R} \left(\frac{N_0 l_0}{A N^* d} - 1 \right) . \tag{36}$$

In Fig. 4, the rates of the four processes, calculated with the parameter values mentioned above, are shown against the normalized power density $1/A$ for pumping through the TE_0 mode. It is seen that for typical values of $1/A$ ($A = 0.024$ for TE_0 at $W = 100$ mW) Raman-induced feeding due to zone-boundary phonons generated after excited-state absorption is strongest.

In the treatment of spatial diffusion in Sec. IIIB, we have taken the local optical feeding to be proportional to $N^*(z)$. To justify this assumption, we return to the $\phi_i(z)$

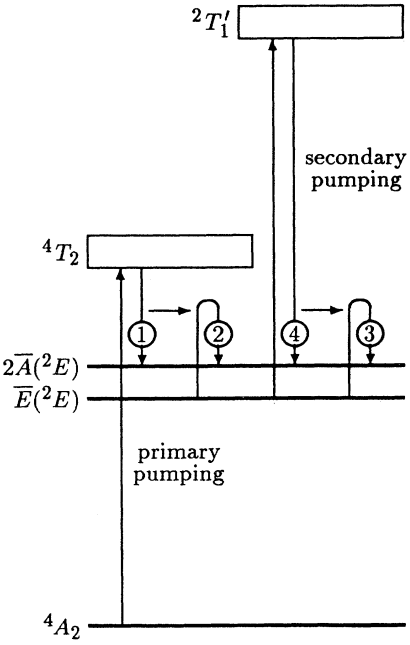

FIG. 3. Schematic representation of the four mechanisms of feeding into $2\overline{A}(^2E)$.

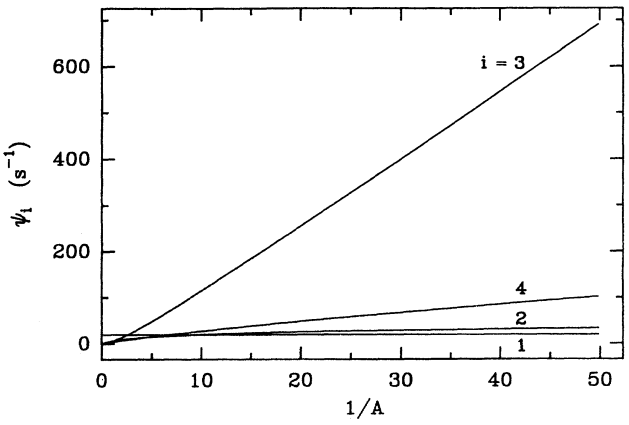

FIG. 4. The contributions ψ_i to the feeding into $2\overline{A}(^2E)$ per excited Cr^{3+} ion vs $1/A$. Conditions apply to the TE_0 mode.

to see that they are indeed proportional to $N^*(z)$, with the exception of $\phi_4(z)$ because it is also dependent on the local power density. The ratio $\phi_4(z)/\phi_3(z)$ is highest at the substrate-film interface, where it is near unity. At greater depth it decreases exponentially with the penetration depth l_0 of the evanescent field. The direct redistribution $\phi_4(z)$, in fact, results in a minor tilting of the distribution $p_0(x)$ towards the substrate-film interface in comparison with Eq. (12), and a correspondingly minor change in the amplitudes a_n in Eq. (10). Equation (14) and the conclusions arrived at in connection with Eq. (18) are, however, not affected.

IV. RESULTS AND DISCUSSION

A. Phonon loss

In the experiments, the laser light was coupled either into the TE_0 or the TM_0 mode. The optical pumping was modulated with an acousto-optical modulator at a frequency of 2.5×10^5 Hz with a duty cycle of 0.5. The decay of the $2\overline{A}(^2E)$ population, as detected via the R_2 luminescence after interruption of the feeding, appeared to be single-exponential. The effective decay times T_{eff} of the R_2 luminescence are presented in Figs. 5 and 6 as a function of the guided-mode power. To determine the latter, the laser power entering the cryostat was measured and corrected for reflection at the helium-prism interface. The coupling efficiency was estimated to be 50%. As a consequence of the logarithmic dependence of N^*d on W, the associated uncertainty in the guided-mode power has no marked effect on the outcome of the analysis below. The standard deviation in T_{eff} amounts to typically 10%.

In Fig. 5, referring to the TE_0 mode, it is seen that T_{eff} is prolonged from the spontaneous decay time $T_d \approx 1$ ns to about 600 ns. After an initial rise, T_{eff} in fact becomes nearly independent of the guided-mode power at this level. Note that this behavior is quite distinct from the flattening out of T_{eff} observed at the high N^*L achieved in the bulk.[2,4] In bulk 700-at.ppm ruby, the notably higher level of about 1.2 μs is attained. For pumping through the TM_0 instead of the TE_0 mode, but under otherwise the same conditions (Fig. 6), T_{eff} is again found to be nearly independent of the guided-mode power, although at a slightly lower level.

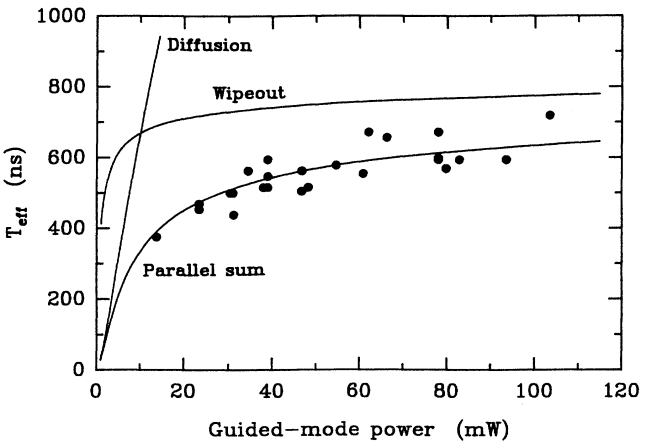

FIG. 5. The decay time of $2\overline{A}(^2E)$ vs guided-mode power following switching off of the optical pumping. The curves represent calculated decay times for wipeout, spatial diffusion, and their parallel sum. The guided mode is TE_0.

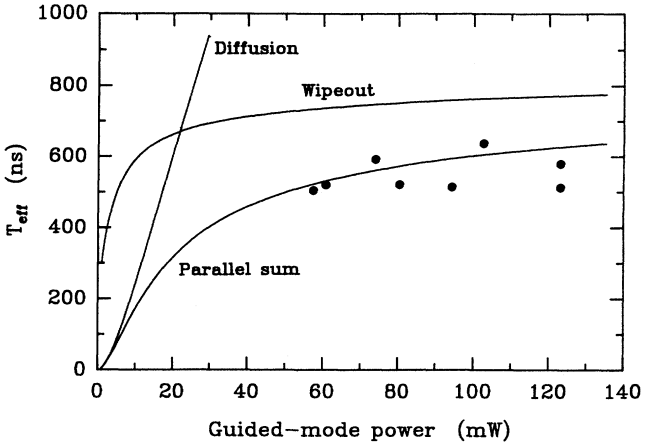

FIG. 6. As in Fig. 5, but for optical pumping through the TM_0 mode.

Before analyzing these results in terms of the theory developed in Sec. III B, it is once more necessary to consider the reflection of phonons at the substrate-film interface. This reflection tends to increase the effective zone thickness for phonons engaged in residual spatial diffusion after a spectral wipeout. Reflection of THz phonons at polished surfaces of various crystalline materials has recently been studied experimentally by Happek, Pohl, and Renk.[20] They found reflection coefficients amounting to $R = 0.80$, virtually independent of the material and further surface treatment. This remarkable insensitivity of R was ascribed to the presence of surface damage layers produced by the polishing. We take $R = 0.80$ at the surface of the ruby substrate, noting that this is an upper limit as it is not known to what depth the damage layers extend, and further neglect any reflection from the film-helium interface. We further point out that in the case of a finite R the increase in effective zone thickness depends on $\Lambda_{\text{el}}(J)$ [cf. Eq. (16)], and thus on the mean number n of elastic scattering events after a frequency displacement that ultimately leads to removal of the phonon from the zone. In our experiments, n averages to the order of 10. However, for J close to J_{crit}, n approaches 100, resulting in an increase in the effective zone thickness by 25% at most. In the calculation of J_{crit} from the criterion Eq. (26), we have nevertheless accounted for this correction by substituting $1.25N^*d$ for

the value of N^*h appropriate to a slab of thickness h.

We now apply the model of Sec. III B to the data in Fig. 5. Two of the curves drawn in Fig. 5 represent the effective decay times for spatial diffusion of resonant phonons, calculated from Eq. (14), and for spectral wipeout, as calculated from Eqs. (22) and (23) in conjunction with the criterion Eq. (26). A third curve shows the parallel sum of these decay times. The parameter values $B = 0.10$ mm and $w_h = 6$ kW/cm^2 were used, combined with the entries in Table I for the TE_0 mode. Furthermore, we set $\alpha = 0.12$ in order to achieve the best fit. The data are indeed well described by phonon escape to the unpumped regions by spectral wipeout in parallel with spatial diffusion. Quite distinct from what one would, at first glance, expect for a zone of small dimensions, however, T_{eff} is found to result primarily from spectral wipeout, with spatial diffusion contributing only one fifth to the total decay. The near independence of T_{eff} on the guided-mode power is caused by the logarithmic dependence of N^*d on W [cf. Eq. (3)] in conjunction with the weak dependence on N^*L that is characteristic of spectral wipeout.[4]

As far as the data in Fig. 6 are concerned, it may be inferred from Table I that the TM_0 mode generates an evanescent field of slightly higher power density than the TE_0 mode, penetrating significantly deeper into the substrate. Its absorption coefficient by Cr^{3+} at 514.5 nm has, however, decreased to 45% relative to that of the TE_0 mode,[18] modifying w_h correspondingly, because the light polarization now is virtually parallel to the c axis instead of perpendicular. Further, the zone width has increased to $B = 0.19$ mm. Taken together, these modifications result in a smaller N^*d than for the case of the TE_0 mode at comparable W. Upon taking due account of these changes, but otherwise with the same parameters, a calculation of the decay times associated with spatial diffusion and spectral wipeout results in the curves presented in Fig. 6. The sum curve again accounts well for the data, essentially confirming the conclusion derived from Fig. 5. Spectral wipeout again turns out to be the dominant relaxation mechanism, although spatial diffusion has gained in importance.

The most noteworthy conclusion of the above analysis is that phonon escape from a submicrometer zone can be described in terms of spatial diffusion and spectral wipeout much like phonon escape from zones of substantially larger size, such as is realized in the bulk. To consider this in somewhat more detail, it is of interest to compare the present result $\alpha = 0.12$ with values for α derived from available bulk measurements but on the basis of the refined wipeout criterion Eq. (26). To this end, we have reanalyzed the data of Ref. 4, which are taken at high N^*L ($\sim 5 \times 10^{16}$ cm^{-2}) in Verneuil-grown 700-at. ppm ruby by modulated optical pumping with an argon-ion laser beam focused down to a waist measuring upwards from 60 μm. Allowing for the cylindrical geometry, we then find $\alpha = 0.14$. Reference 21 presents data taken in another crystal from the same boule as our ruby for $N^*L \sim 10^{15}$ cm^{-2}. This value is comparable to N^*d attained in the present waveguide experiment, but is made up of a much larger radius $R = 100$ μm and a much lower $N^* \sim 10^{17}$ cm^{-3}. A fit of our refined model to these data, with due account of the elongation of T_{eff} by the factor $1+\rho\Delta\nu/N^*$, results in an excellent description for $\alpha = 0.18$. The bulk data thus show that in extended zones of comparable N^*L, α is somewhat larger than in the present waveguide experiments, and that α decreases with increasing N^*L.

At this point, we recall that the parameter α originates from a reduced coupling between the resonant phonon packet and the type-II Cr^{3+} ions as a result of broadening of the $\overline{E}(^2E)-2\overline{A}(^2E)$ transitions of the ions with increasing pair exchange. The minimum frequency shift undergone by a phonon upon scattering from type-II ions, J_{crit}, decreases quite steeply with decreasing N^*L. We find $J_{\text{crit}} = 0.11$ cm^{-1} at $N^*L = 5 \times 10^{16}$ cm^{-2}, reducing to $J_{\text{crit}} = 0.013$ cm^{-1} at $N^*L = 1.5 \times 10^{15}$ cm^{-2}. Accordingly, the type-II transitions on the average become narrower, and α correspondingly increases, towards lower N^*L, in qualitative agreement with the bulk experiments. Further, an important feature of the waveguide experiments is that the ground state is significantly depopulated. Indeed, a depletion of the ground state invokes an increase in T_{eff}, or in the present context a decrease in α, as has previously been observed by Meltzer, Rives, and Egbert.[2] Under these conditions, it is likely that both Cr^{3+} ions constituting an exchange-coupled pair are excited to $\overline{E}(^2E)$. In terms of the exchange splitting J, therefore, the $\overline{E}(^2E)-\overline{E}(^2E)$ exchange apparently is weaker than the $\overline{E}(^2E)-{}^4A_2$ exchange. Indeed, if the parameter J_0 is reduced by a factor of 4, the model provides an excellent account of the waveguide data for $\alpha = 0.18$.

B. Feeding

The feeding into $2\overline{A}(^2E)$ can be monitored experimentally by measuring the intensity of the R_2 luminescence. The time-averaged feeding into $2\overline{A}(^2E)$ $\langle\Phi\rangle$ balances the decay, which equals $\langle N_{2\overline{A}}\rangle/T_{\text{eff}}$. In Fig. 7, the latter ratio is plotted versus the guided-mode power. At first glance, the data show an almost linear dependence, but linear extrapolation to zero guided-mode power results in a negative intercept with the vertical axis. This is in contrast with conventional bulk experiments, and is related to the fact that no substantial region of near saturation can be maintained at very low guided-mode powers.

To compare the theory of Sec. III C with the data, we calculate the time-averaged feeding $\langle\Phi\rangle = \sum_{i=1}^{4}\int_0^\infty \phi_i(z)dz = \sum_{i=1}^{4}\psi_i N^*d$ (cf. Fig. 4), which results in the curves in Fig. 7. The data are well described by these curves without any adjustment of the parameters specified in Sec. III C, apart, of course, from an overall scaling factor, which is taken to be identical for the TE_0 and TM_0 data. For the guided-mode

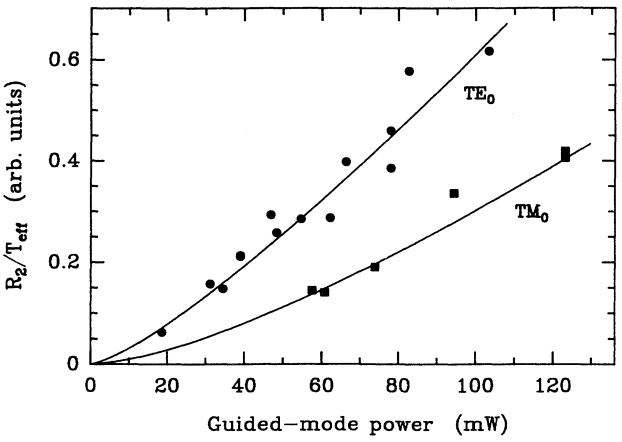

FIG. 7. The ratio of the time-averaged R_2 intensity and the relaxation time for pumping through the TE_0 and TM_0 modes. Curves represent the total feeding according to Sec. III C.

powers where data are available, the feeding is dominated by Raman processes induced by excited-state absorption. Note that in conventional bulk experiments, excited-state absorption at a wavelength of 514.5 nm is almost negligible.[17] The striking contrast is due to the extremely high excited-ion and power densities in our experimental situation. Indeed, without the presence of excited-state absorption, the signal levels would have been so low as to render the experiments impossible.

C. Excitation of Cr^{3+} in the bulk

In the analysis of the phonon dynamics in a small-geometry experiment such as the present one, one should be on the alert for residual excitation of Cr^{3+} in the bulk because of the much larger typical length scale. By far the most important source of bulk excitation is reabsorption of the R_1 luminescence emanating from the excited zone, resulting in a "blanket" of excited Cr^{3+} ions. The thus generated bulk N^*, N_b^*, can be estimated from simple considerations. The rate at which R_1 photons are emitted by Cr^{3+} in the excited zone amounts to N^*d/τ_R per unit area, approximately half of which enters the bulk below the zone. Here, the phonons travel an average distance $\frac{1}{2}\Lambda_R$ in the z direction before being reabsorbed, with $\Lambda_R \sim 250$ μm the mean free path for R_1 photons in 700-at. ppm ruby. Balancing feeding and decay, we then find $N_b^* \approx N^*d/\Lambda_R$. For the experiment of Fig. 5, this would yield $N_b^* \approx 6 \times 10^{16}$ cm^{-3} immediately below the excited zone. Beyond the immediate vicinity of the excited zone, N_b^* would drop inversely proportionally to the distance, were it not that the R_1 photon engages in a diffusive motion from Cr^{3+} to Cr^{3+} until it escapes. Furthermore, reflection of the luminescence at the sample boundaries enhances N_b^*, and modifies its distribution.

To investigate these effects further, we resorted to a Monte Carlo computer simulation. The excited zone is represented by a uniform rectangular slab positioned at the sample surface. The sample has a thickness of 1 mm and a width of 2 cm. The simulation tracks the itinerary of phonons randomly generated over the slab, marking the location of the interrupting Cr^{3+} ions. The presence of a film on the sample is neglected. The problem is, furthermore, made two dimensional by multiplying the mean free path by a factor $\pi/4$. In each step, a random number decides the direction of travel, and a second random number draws the distance to be covered to the next reabsorption from the stochastic distribution of distances appropriate to an intensity dropping exponentially with the mean free path. If a photon hits a sample boundary, the reflection coefficient relevant to the angle of incidence is calculated while averaging over the σ and π polarizations, and a third random number decides whether the photon escapes or is specularly reflected. If a photon exits through the upper face of the sample, the location of the escape is also recorded. In Fig. 8, the number of photons that leave the sample through the upper sample surface is compared with the R_1 luminescence measured while scanning along the sample surface perpendicularly to the guided laser light. Good agreement is found. In the simulations a photon suffers, on the average, approximately 12 interruptions before escaping from the sample. Figure 9 shows a simulated N_b^* distribution as a function of the depth below the excited zone. The latter is given the typical width 100 μm and thickness 0.5 μm. Here, N_b^* is expressed as a fraction of the N^* in the zone, which approximates $N_0 = 3 \times 10^{19}$ cm^{-3}. From the simulations, N_b^* in the immediate vicinity of the zone is seen to be about three times higher than that calculated ac-

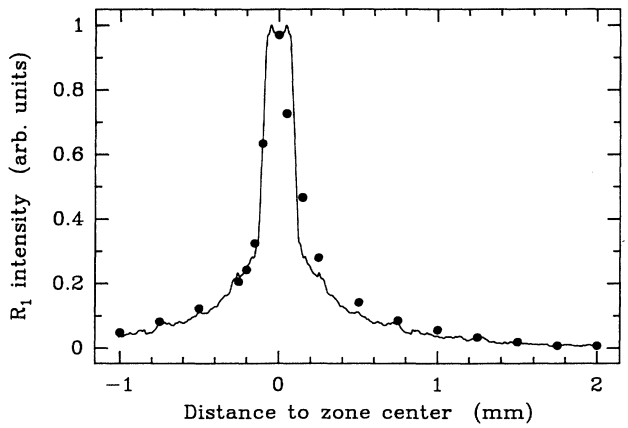

FIG. 8. The measured R_1 luminescence vs the lateral distance to the center of the excited zone. The zone is pumped through the TM_0 mode. The curve represents the R_1 luminescence as calculated in a computer simulation for a zone of 200×0.8 μm^2 cross section, convoluted with the instrumental profile of the detection.

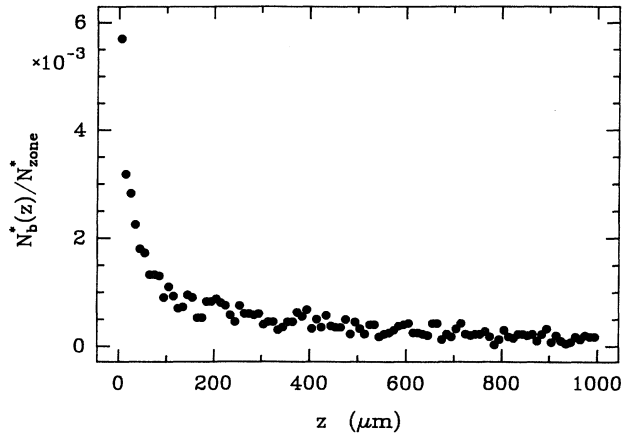

FIG. 9. Results of a computer simulation, relative to N^* in the zone, of the bulk excited-ion concentration N_b^* caused by multiple reabsorption of the R_1 luminescence, vs the depth below the zone center. Zone dimensions are $100 \times 0.5\ \mu m^2$.

cording to the simple estimate above. Further, N_b^* drops somewhat more slowly than it would according to the reciprocal distance.

When estimating the contributions to the luminescence from the blanket of excited Cr^{3+} beyond the actual excited zone, we first note that the blanket by itself does not contribute to the R_2 luminescence. Scattering of zone-boundary phonons emanating from the excited zone (cf. Sec. III C), however, may result in excitation to $2\overline{A}(^2E)$ and R_2 luminescence. The density of these phonons drops with $1/r$, and the resulting contribution to the R_2 luminescence is estimated to be 10% at most. The blanket, however, contributes significantly to the R_1 luminescence. The integral of N_b^* over the depth of the sample amounts to $\approx 1.1N^*d$, indicating that about half of the R_1 luminescence originates from the blanket. For this reason, the absolute rate of the R_2 luminescence instead of the ratio R_2/R_1 was entered into the analysis of our experiments. With regard to 29-cm^{-1} phonons escaping from the excited zone, it is noted that they "see" the blanket as virtually transparent, since in their release from the zone by wipeout they have undergone a substantially larger frequency shift than the shift required for wipeout in the blanket. In summary, the above considerations indicate that the blanket has only minor effects on our results.

V. CONCLUSIONS

We have shown that an optical waveguide permits the study of the dynamics of high-frequency phonons in active zones of submicrometer dimension in ruby crystals. In comparison with previous experiments in bulk ruby, the zone is contracted only in one dimension so that sufficient luminescent intensity could still be collected. The technique furthermore achieves a high power density of the laser light and an extreme excited-ion concentration in the excited zone. As a result, optical pumping is seen to be greatly enhanced by processes associated with excited-state absorption from $\overline{E}(^2E)$, whereas these processes are negligible in the bulk at the light frequency used.

A major conclusion of the present work is that L is a parameter relevant to phonon loss at any N^*. The chief mechanisms of phonon loss considered are spatial diffusion towards the zone boundary and spectral wipeout. A submicrometer zone of excited Cr^{3+}, then, appears not to behave very differently from an extended zone for comparable N^*L. Resonant high-frequency phonons are, in fact, imprisoned in submicrometer zones of nearly saturated excited Cr^{3+} concentrations. From a rigorous calculation, spatial diffusion turned out to be relatively ineffective, as it is in the case of extended zones, despite the small distances to be covered until escape. For an estimate of phonon loss by wipeout, we have successfully relied on an approximate analytical model for one-site Raman scattering by weakly exchange-coupled Cr^{3+} pairs, which provides frequency shifts of the order of the phonon transition width. However, the criterion for wipeout needed to be refined in order to apply to the somewhat lower N^*L encountered here. The model then gives a good account of the effective decay time after interruption of the optical pumping as a function of guided-mode power. The broadening parameter α is found to equal the values in the bulk at high N^*L, although a larger α is anticipated from the smaller average frequency shift needed for wipeout. This is probably due to a reduction of the exchange parameter upon excitation of both Cr^{3+} ions in a pair.

ACKNOWLEDGMENTS

The authors thank C. M. M. Denisse and ASM in Bilthoven, The Netherlands, for providing the siliconoxynitride films. The work was financially supported by the Netherlands Foundation Fundamenteel Onderzoek der Materie (FOM) and the Nederlandse Organisatie voor Wetenschappelijk Onderzoek (NWO).

[1] For a review, see K. F. Renk, in *Phonon Scattering in Condensed Matter*, edited by W. Eisenmenger, K. Laßmann, and S. Döttinger (Springer-Verlag, Berlin, 1984), p. 10.
[2] R. S. Meltzer, J. E. Rives, and W. C. Egbert, Phys. Rev. B **25**, 3026 (1982).
[3] S. A. Basun, A. A. Kaplyanskii, S. P. Feofilov, and V. L. Shektman, Fiz. Tverd. Tela (Leningrad) **25**, 2731 (1983) [Sov. Phys. Solid State **25**, 1570 (1983)].
[4] R. J. G. Goossens, J. I. Dijkhuis, and H. W. de Wijn, Phys. Rev. B **32**, 7065 (1985).
[5] S. Majetich, R. S. Meltzer, and J. E. Rives, Phys. Rev. B **38**, 11 075 (1988).

[6] H. Kogelnik and V. Ramaswamy, Appl. Opt. **13**, 1857 (1974).
[7] P. K. Tien, Rev. Mod. Phys. **49**, 361 (1977).
[8] *Integrated Optics*, Vol. 7 of *Topics in Applied Physics*, 2nd ed., edited by T. Tamir (Springer-Verlag, Berlin, 1979).
[9] J. E. Midwinter, IEEE J. Quantum Electron. **QE-6**, 583 (1970); J. H. Harris, R. Schubert, and J. N. Polky, J. Opt. Soc. Am. **60**, 1007 (1970); P. K. Tien and R. Ulrich, *ibid.* **60**, 1325 (1970); R. Ulrich, *ibid.* **60**, 1337 (1970); T. Tamir and H. L. Bertoni, *ibid.* **61**, 1397 (1971).
[10] J. Crank, *The Mathematics of Diffusion*, 2nd ed. (Oxford University Press, London, 1975), p. 47.
[11] L. E. Reichl, *A Modern Course in Statistical Physics* (University of Texas Press, Austin, 1980), p. 460.
[12] H. S. Carslaw and J. C. Jaeger, *Conduction of Heat in Solids* (Oxford University Press, London, 1947), p. 13.
[13] S. K. Lyo, Phys. Rev. B **3**, 3331 (1971).
[14] It is shown in Ref. 4 that spectral wipeout is not essentially modified by adopting other reasonable dependences of J on the distance.
[15] M. J. van Dort, M. H. F. Overwijk, J. I. Dijkhuis, and H. W. de Wijn, Solid State Commun. **72**, 237 (1989).
[16] M. H. F. Overwijk, J. I. Dijkhuis, and H. W. de Wijn (unpublished).
[17] R. J. G. Goossens, J. I. Dijkhuis, and H. W. de Wijn, Phys. Rev. B **32**, 5163 (1985).
[18] W. M. Fairbank, Jr., G. K. Klauminzer, and A. L. Schawlow, Phys. Rev. B **11**, 60 (1975).
[19] J. G. M. van Miltenburg, J. I. Dijkhuis, and H. W. de Wijn, *Phonon Scattering in Condensed Matter*, Vol. 51 of *Springer Series in Solid-State Sciences*, edited by W. Eisenmenger, K. Laßmann, and S. Döttinger (Springer-Verlag, Berlin, 1984), p. 118.
[20] U. Happek, R. O. Pohl, and K. F. Renk, in *PHONONS 89*, edited by S. Hunklinger, W. Ludwig, and G. Weiss (World Scientific, Singapore, 1990), p. 925.
[21] M. J. van Dort, J. I. Dijkhuis, and H. W. de Wijn, Phys. Rev. B **41**, 8657 (1990).